Evaluating the Role of Microclimate change in Urban Heat Island using Mobile Measurement

Yichen Yang, Class of 2020, MESc, School of Forestry and Environmental Studies

Academic Advisor: *Xuhui Lee* (xuhui.lee@yale.edu)

1. Introduction

1.1. The origin of UHI issue

As a result of urbanization, anthropogenic climate change in urban areas has become one of the major climatic crises mankind must face besides global climate change [1]. Urban Heat Island, hereinafter UHI, is the rising temperature in urban area as opposed to rural area, increasing heat stress and thus exacerbating heat-related mortality [1-3]. Therefore, actions to mitigate UHI intensity have become urgent, which should be based on profound understanding of UHI mechanism. However, our understanding of how the UHI comes into being is still insufficient, especially in the thermal process underlying the formation of Urban Heat Island (UHI).

1.2. Observing the UHI

1.2.1 The application and limitation of technologies used for observation

To measure the intensity UHI, the *in-situ* measurement and the satellite remote sensing technology are widely used because of satisfying spatial and temporal representativeness [4]. However, the *in-situ* network cannot be installed at street level in the cities and the typical high spatial resolution of satellite image (e.g., 30 m, from Landsat 7 ETM+) is still limited for very local observation. In short, both of the methodologies are not capable of capturing the details of temperature at the street floors.

1.2.2 The importance of street-level UHI observation

Why is the street-level UHI so important? Prominent change of building geometry, vegetation fraction, underlying material, and illumination can create several distinct microclimates even within a small area [5]. As a result, the street-level UHI at local scale is more sensitive to the surrounding environment and is controlled by a more complicated mechanism than a larger scale. On top of this, the air temperature is a more unpredictable variable compared to surface temperature because it has to do with the ambient thermodynamic condition, and is scale-dependent at street-level [6]. Therefore, the street-level Air Urban Heat Island (AUHI) is a key to the profound understanding of how microclimate change impacts UHI intensity.

1.2.3 The potential of mobile measurement in observing street-level AUHI

To acquire high-resolution data of AUHI intensity at street-level, mobile measurement plays a key role here. Mobile measurement is using a car or a bike as the platform for the sensors to collect data along the transect of the city [7, 8].

1.2.4 The comprehensive consideration of thermal comfort indices in exploring UHI

Dry bulb temperature is used widely in UHI studies because it's a straight representative of urban climate. However, for comprehensive consideration which seeks to model the exposure of real human skin to urban climate, more complicated thermal comfort indices should be considered (Francisco Gomez). For example, wet bulb temperature is a good proxy of thermal comfort because it describes how the sweating human skin responds to urban heat by combining the dry bulb temperature with air humidity.

1.3 Research questions

In this research, I will specifically answer the following questions by means of mobile measurement: (1) How does the street-level AUHI vary spatially and temporally in terms of both dry bulb temperature and wet bulb temperature? How does the distribution of wet bulb temperature differ from that of dry bulb temperature? (2) How does the street-level AUHI relate to the microclimate changes (e.g., tree canopy cover and building morphology). How different are the relations between dry bulb temperature and wet bulb temperature? (3) Whether urban humidity will be persistently lower than in the surrounding rural land and to what degree the humidity change can reduce the heat stress on urban residents.?

2. Research hypothesis

2.1 H1: The central area of the city is warmer than the off-center area. The spatial distribution of street-level AUHI changes with weather condition. Wet bulb temperature is less spatially variable than dry bulb temperature.

2.2 H2: The more tree canopy cover, the weaker the street-level AUHI. The built-up area doesn't have the strongest AUHI because the building shadow.

2.3 H3: Urban humidity will not be persistently lower than in the rural land. The wet island effect can take place when there exist stable sources of moist.

3. Data and methods

3.1 Study area

This research will be carried out in New Haven, Connecticut, U.S. This city is selected because its surrounding typical rural area is located within 3 miles of the heavily built-up region. The contrast of land cover and city geometry is distinct. A single mobile measurement along the finally determined city transect, from the urban core to the typical rural environment, can be done in 20 minutes.

3.2 Experimental settings

3.2.1 Experimental background

The primary measurements were carried out in August 12, 2019. 15 volunteers were recruited in advance from the Summer Orientation Modules (MODs) of Yale School of Forestry & Environmental Studies (https://environment.yale.edu/mods). Additional biking data were been collected continuously from September to December.

3.2.2 Instruments

The sensor to be attached on a bike is Smart-T (Figure1), an air temperature and relative humidity (Ta/RH) sensor developed and produced by Jiangsu Radio Scientific Institute Corporation, Jiangsu Province, China (see specification in Table 1). Smart-T communicates with a mobile phone and sends the logged Ta/RH data via Bluetooth signal. The GPS information of each data point is acquired straight from a mobile phone's GPS module.

(a) (b)

Figure 1. (a) The Smart-T bike sensor. (b) How the sensor is attached on a bike for mobile measurement.

Table 1. Specification of Smart-T bike sensor

	Ta Sensor	RH Sensor
Range	-40 - 60°C	10-90%
Accuracy	±0.3°C	±2%
Response Time	~8s	
Standby power consumption	0.06 mW	
Typical power consumption	0.36 mW	
Max power consumption	1.38mW	
Operating temperature range	-20 - 60°C	
Ingress Protection Rating	IP65	

Weight with batteries	63g
Height	85mm
Radiation shield material	ABS-like resin

To derive the temperature anomaly which represents the UHI intensity reasonably, three mini-weather stations, HOBO External Temperature/RH Sensor Data Logger (https://www.onsetcomp.com/products/data-loggers/mx2302a), were set up in different typical urban environments, including tree shade (Figure 2a), open area (Figure 2b) and building shade (Figure 3c). They are meant to provide referential background measurement of Ta and RH as the mobile measurement is going on.

(a) (b) (c)

Figure 2. The setting of referential background measurement: (a) HOBO sensor in tree shade. (b) HOBO sensor in open area. (c) HOBO sensor in building shade. The three HOBO sensors are set in different typical urban environments but still close enough to represent the same region.

3.2.3 Biking route

The mobile measurements were repeated on the same group of bike routes (Figure 3) in order to make the data from different days comparable. The routes are selected to cover different typical urban environments as selected for the HOBO sensors. In the Figure 3, several urban parks, such as New Haven Green and Wooster Square, were chosen as regions with massive tree canopy cover. There are other chosen urban parks like Dover Beach and Criscuolo Park which are not dominated by tree canopy cover but are in the vicinity of the water. The region ① was the only area with dense buildings, and so with heavy blockage of buildings to solar radiation.

Figure 3. The bike routes (blue lines) used to repeat the mobile measurement. The labeled places on the map represent different landscapes: ① built-up area, ② New Haven Green, ③ DeGale Field, ④ Wooster Square, ⑤ Criscuolo Park, ⑥ Jocelyn Square Park, and ⑦ Dover Beach. The “S” region is the starting point of all the measurements. All the regions from ② to ⑦ are urban parks with either dominant tree canopy cover or grassland.

3.3 Sensor calibration

Prior to the formal experiment, all the sensors, including the Smart-T bike sensors and the HOBO sensors, need to be calibrated to solve the systematic error in measurement. Fan Test is proved to be a solid methodology to do the inter-comparison among the sensors. It is using two fans promoting ventilation in opposite directions, assuming that the air temperature at the same horizontal level in the space between the fans is homogeneous. Therefore, if all the sensors are placed on a table within that space (Figure 4), the difference between the sensor readings at the same time should be cause by the systematic error that comes with the sensors.

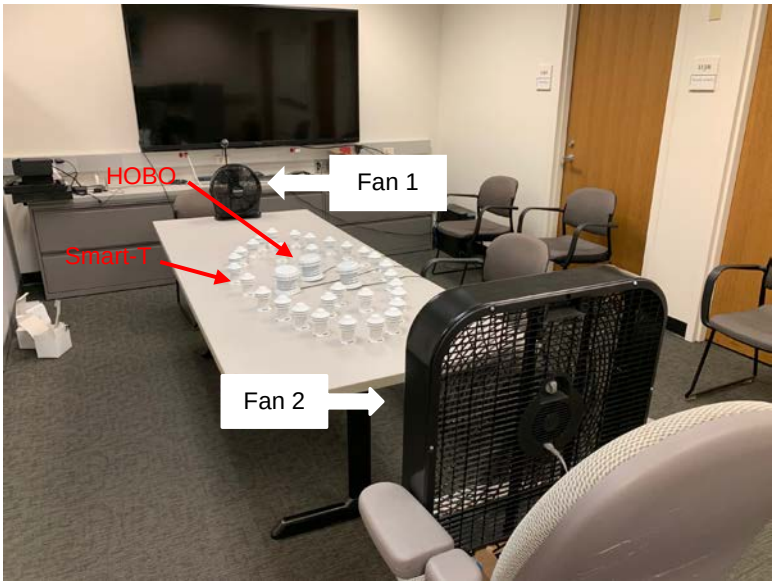

Figure 4. The layout of the Fan Test calibration method. Fan 1 and Fan 2 are used to promote ventilation to create isothermal field in the space between them. The sensors, including Smart-T's and HOBO's, are placed on the table the way that minimizes the chance that a sensor blocks the air flowing through the others. The HOBO sensors are surrounded by the Smart-T sensors.

The Fan Test took about 4 hours. The HOBO sensors were logging data throughout the whole period, while the Smart-T sensors were connected in turn to a phone for data logging, each with a 5-minutes-window. Given the overlap of the measurements among the sensors, we are able to see how the sensors perform differently when actually measuring in the same Ta/RH environment. Figure 5 gives intuitive results of the inter-comparison. It shows that during the short window of 5 minutes, the Ta/RH variation trends of the Smart-T and HOBO sensors are quite consistent. This proved that the Fan Test is a valid method to capture the systematic error between sensors without being affected by the temporal variability of the variables.

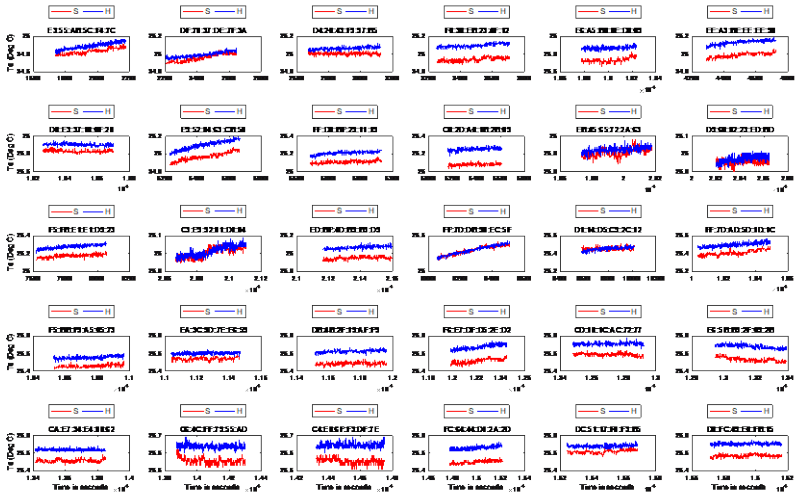

(a)

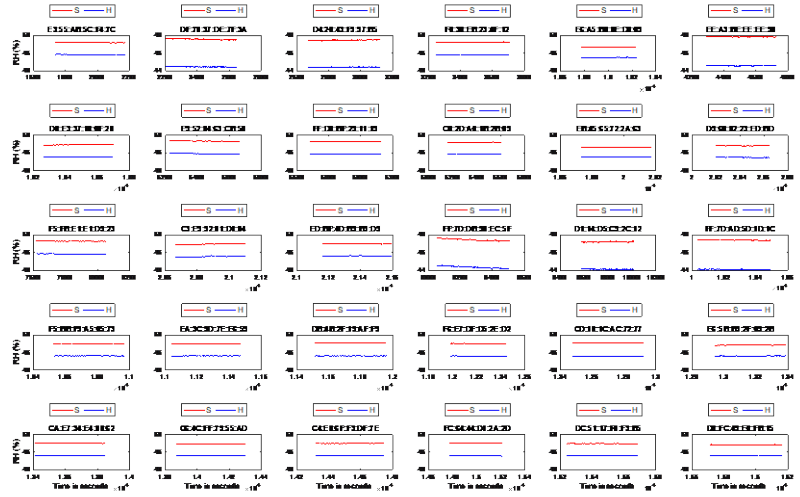

(b)

Figure 5. The inter-comparison between all the Smart-T sensors and a chosen HOBO sensor as the reference. (a) The difference of Ta values. (b) The difference of RH values. Red line (S) is the time series of Smart-T sensor and the blue line (H) is the HOBO sensor. Each graph is labeled with the name of the individual Smart-T sensor being tested(The name is in the form of a Bluetooth name, such as “E3:55:AB:5C:F4:7C”). All the sensors were logging with a 1-second-interval.

To solve the systematic error in terms of Ta and RH value, we computed the Root Mean Square (RMS) and the Mean Error (Offset) for the Smart-T sensors based on their 1-second-interval time

overlap with the HOBO sensor. RMS is used to assess the error (Equation 1), and Offset is used to reduce the error and then calibrate the sensors (Equation 2).

$$\mathrm{RMS} = \sqrt{\frac{1}{n}\sum(V_H - V_S)^2} \qquad \text{Equation 1}$$

$$\mathrm{Offset} = \frac{1}{n}\sum(V_H - V_S) \qquad \text{Equation 2}$$

$$\mathrm{H} = \mathrm{S} + \mathrm{Offset} \qquad \text{Equation 3}$$

As explained by the Equation 1 and 2, RMS considers the error regardless whether it's positive ($V_H > V_S$) or negative ($V_H < V_S$), where V_H and V_S are the variable measured by HOBO sensor and Smart-T sensor, respectively. V can be any variable but is specifically Ta or RH in this case. Equation 3 shows that the Ta/RH values from a Smart-T sensor (S) during the mobile measurement will be adjusted to the level of the reference HOBO sensor (H) by adding the Offset to it. Since only one of the HOBO sensors was chosen as the reference, the RMS and Offset of other HOBO sensors compared to the reference sensor will also be computed. The RMS and Offset for all the sensors are listed below (Table 2).

Table 2. The RMS and Offset of Ta/RH value for all the sensors. (b) The RMS and Offset of RH for all the sensors. The reference sensor is named HOBO 83, thus the rest of HOBO sensors to be calibrated are HOBO 84 and HOBO 85. The unit is "Deg C" for Ta and "%" for RH.

Device Name	RMS (Ta)	Offset (Ta)	RMS (RH)	Offset (RH)
F47C	0.06	0.06	3.41	-3.41
7F3A	0.04	0.03	3.12	-3.12
97B5	0.06	0.06	3.05	-3.05
4F12	0.16	0.16	3.60	-3.60
D009	0.14	0.14	2.93	-2.93
EE98	0.14	0.14	3.27	-3.27
0F28	0.08	0.07	3.48	-3.48
CB50	0.13	0.13	3.55	-3.55
1119	0.10	0.10	3.54	-3.54
2B09	0.18	0.17	3.36	-3.36
2A63	0.03	0.01	2.75	-2.75
EDBD	0.03	0.02	3.28	-3.28
D923	0.10	0.10	3.59	-3.59
D184	0.02	0.01	3.51	-3.51
B3D9	0.12	0.12	3.46	-3.46
EC5F	0.02	0	3.07	-3.06

2C12	0.03	0	3.06	-3.06
1D1C	0.09	0.09	3.30	-3.30
0573	0.10	0.10	3.38	-3.38
E659	0.07	0.06	3.34	-3.34
AFF9	0.14	0.14	3.60	-3.60
2ED2	0.16	0.16	3.52	-3.52
7277	0.12	0.12	3.68	-3.68
092B	0.15	0.15	3.06	-3.06
8862	0.13	0.13	3.53	-3.53
55AD	0.08	0.08	3.28	-3.28
DF7E	0.09	0.09	3.48	-3.48
2A2D	0.16	0.16	3.53	-3.53
F3B5	0.07	0.06	3.47	-3.47
FB15	0.14	0.13	3.15	-3.15
HOBO84	0.03	-0.02	0.33	0.32
HOBO85	0.05	0.05	0.05	0.02

3.4 Deriving the UHI intensity

To derive the AUHI intensity from the data collected, the average value of HOBO data needs to be subtracted from the Smart-T data at the same time point (see Equation 4 and 5).

$$\Delta T_d = T_{dS} - (T_{dH83} + T_{dH84} + T_{dH85})/3 \quad \text{Equation 4}$$

$$\Delta T_w = T_{wS} - (T_{wH83} + T_{wH84} + T_{wH85})/3 \quad \text{Equation 5}$$

ΔT_d and ΔT_w are the AUHI intensity in terms of dry bulb temperature and wet bulb temperature, respectively. T_{dS} and T_{dH} are the measured dry bulb temperature values from Smart-T sensor and HOBO sensor, respectively. The numbers following T_{dH} are the ID's of individual HOBO sensors. The same rule is applied to the annotations of wet bulb temperature.

Wet bulb temperature can be calculated using the equations below:

$$C_p(T_d - T_w) = L_v(s_w - s_d) \quad \text{Equation 6}$$

$$s_v = \frac{\varepsilon e_v}{P_d}, \varepsilon = \frac{R_d}{R_v} \quad \text{Equation 7}$$

$$e_v^* = 6.11 \times 10^{(\frac{7.5 \times T_d}{237.3 + T_d})} \quad \text{Equation 8}$$

$$e_v = e_v^* \times RH \quad \text{Equation 9}$$

Equation 6 relates dry bulb temperature (T_d) to wet bulb temperature (T_w) using the parameters C_p, specific heat of air at constant pressure (1004 J kg^{-1} K^{-1}), L_v, latent heat of vaporization (2466 J g^{-1} at 15 °C), s_d water vapor mass mixing ratio for dry bulb temperature, and s_w, saturation water vapor mass mixing ratio for wet bulb temperature. Equation 7 introduces how the general water vapor mass mixing ratio s_v can be calculated using e_v, water vapor pressure, with ε, the ratio of ideal gas constant of dry air to ideal gas constant of water vapor. Since the water vapor pressure needs to be derived from Equation 8 (Magnus-Tetens equation) and 9, s_w is a function of wet bulb temperature (T_w). As a result, Equation 6 has to be solved numerically to get a solution to T_w.

3.5 Other auxiliary dataset

3.5.1 Landcover data and the method of scale-dependency

To examine how the AUHI relates to the surrounding environmental indices, a reliable landcover data is needed to define these indices. The tree canopy/classification data of New Haven County (Jarlath P. M. O'Neil-Dunne) is a GIS raster layer (3-feet resolution) with several landscape categories including tree canopy, grass/shrub, bare soil, water, buildings, roads/railroads, and other paved areas. It is classified using the Connecticut 2016 LiDAR/orthoimagery data.

3.5.2 Building shadow faction layer

To model the building shadow in the city, the high-resolution Digital Surface Model (DSM) is required. Fortunately, the DSM layer can be converted from the Connecticut 2016 LiDAR data, the same data source of the landcover data. The LiDAR dataset comes with the first order classification of ground and non-ground cloud points. Interpolating the ground point and converting them to a raster layer in ArcMap, we acquired the bare earth DSM, or in other words, the Digital Terrain Model (DTM). Through the same workflow, we can generate the DSM of full objects in the city by considering both the ground and non-ground points. The landcover data can tell precisely where the “Building” pixels are, so that the building height can be extracted by subtracting the DTM from the DSM for only the building pixels. Adding the Building height pixels back to the DTM, we created a DSM layer with only the variability of bare earth and buildings: other objects above the ground like the trees are not considered. This allowed us to generate a layer of building shadow by applying the tool “Hillshade” to the building-only DSM layer in ArcMap. The solar angle parameters, Elevation and Azimuth, are determined by the approximate time of the mobile measurement.

3.5.3 Sky View Factor layer

In addition to the building shadow patter, Sky View Factor (SVF) is believed to be a more generalized and traditional index to represent the building morphology. SVF is the portion of the sky area that can be seen by an observer on the street. Since the view of the observer is partly blocked by the surrounding obstacles, i.e. buildings, the lower the SVF, the higher the degree of building

folding. As SVF is reasonably correlated with building shadow fraction during the daytime, it enables a profound understanding of the heating from building energy storage in the nighttime. The GIS technology provides a new opportunity to compute SVF for not only a limited number of observation points, but also a raster layer with high resolution for a region. Applying the “Hillshade” tool to the building-only DSM with different elevation angles, it’s possible to quantify the portion of time in a day a single pixel is illuminated or not. Adding up the portions for all the azimuth angles will generate the Building View Factor (BVF). The SVF is calculated by subtracting BVF from unity. This raster-based method produces SVF of all the pixels in an extent simultaneous, dramatically reducing the time for computing.

3.6 Spatial analysis method

To build the connection between the measurements and these landscapes, the method of scale-dependency from Ziter (2019) was applied [6]. As recommended in Ziter’s work, the street-level temperature is most significantly correlated to the average environmental indices (portion of area) within a 60-90 m buffer around the measuring point, given the intuition that 60-90 m is a typical building cluster size in the city. Here in our work, 90-meter scale is chosen.

4. Results and preliminary discussion

4.1 General statistical patterns

Considering that the clear sky ensures that the ground surface is fully illuminated, so the shadow pattern becomes the most prominent for the area where the sunlight is heavily blocked by the buildings. Therefore, the preliminary discussion is on the August 12 data, data collected under clear sky condition.

By looking at the temperature maps in Figure 6, we can discover that for both the dry bulb temperature and wet bulb temperature the AUHI intensity is stronger in urban core than in the off-center area. The temperature dropped drastically as the cyclists moved eastward to Criscuolo Park and Dover Beach (Figure 3). For the area with massive tree cover, the AUHI intensity also decreased. However, the urban core was far from the warmest. On the contrary, the hot spots appeared more in the peripheral regions, which are still urban but less built-up than the urban core. This may relate to the cooling effect of building shadow. The spatial variability of AUHI intensity is weaker for wet bulb temperature than for dry bulb temperature. This is related to the nature of wet bulb temperature, for which the cold but humid area could be warmer than the warm but dry area after the converting dry bulb temperature to wet bulb temperature.

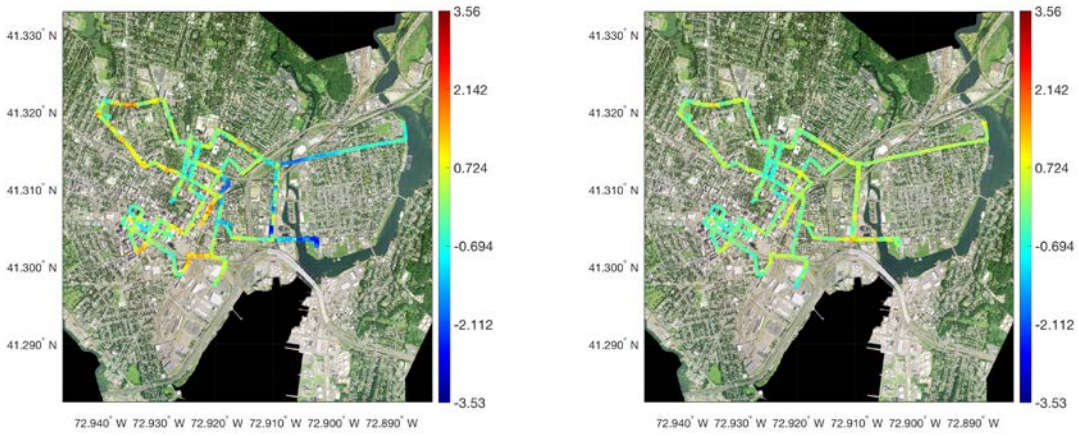

(a) (b)

Figure 6. The temperature maps (with Deg C as the unit) of the data collected on August 12. (a) The AUHI intensity based on dry bulb temperature. (b) The AUHI intensity based on wet bulb temperature.

To investigate the relationship between AUHI intensity and the environmental indices, Figure 7 shows that we can hardly claim a significant correlation between dry bulb AUHI intensity and tree canopy or building shadow. However, the wet bulb AUHI intensity seems to decrease as these two indices increase.

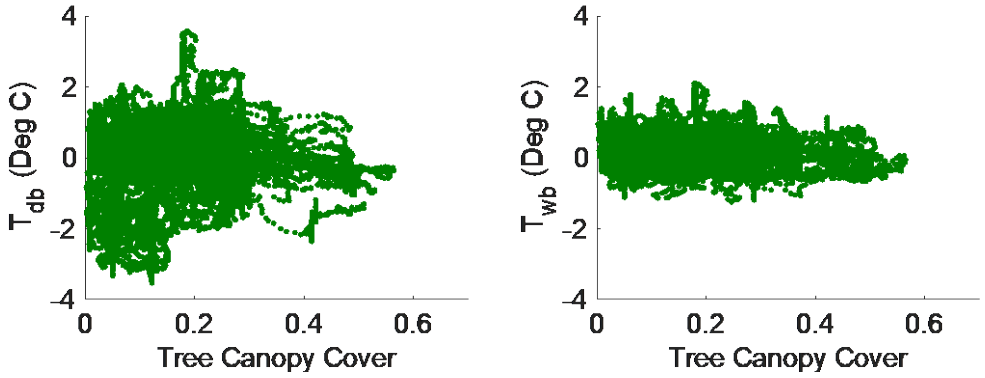

(a) (b)

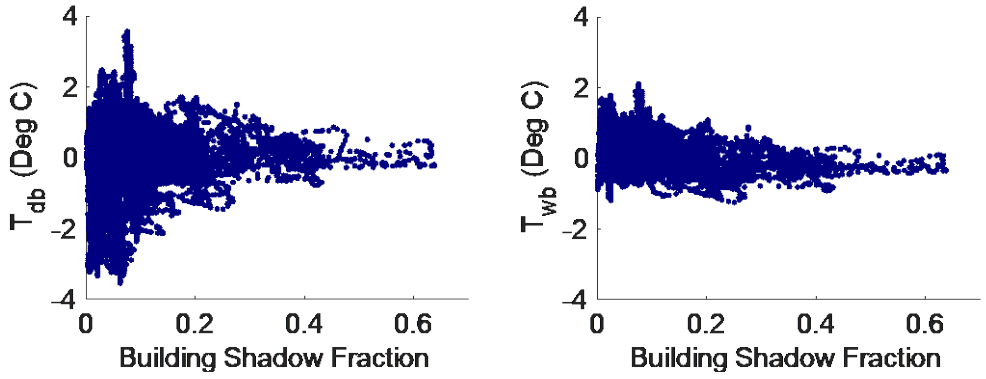

(c) (d)

Figure 7. The scatterplot between the environmental indices and the AUHI intensity in terms of dry bulb temperature, (a) and (c), and wet bulb temperature, (b) and (d). (a) and (b) are for tree canopy cover, and (c) and (d) are for building shadow fraction.

The scatterplots for dry bulb AUHI in Figure 7 look noisier, which is obviously due to some extreme cold spots on the temperature map Figure 6a. We are interested in what the driven force is for these abnormal cold spots. By calculating the difference of water vapor pressure between Smart-T sensors and HOBO sensors, we can relate the water vapor anomaly to the dry bulb temperature. Strong negative correlation between these two factors are seen, which indicates further that the cold spots are also the “humid spots”. Figure 9 shows that the humidity histogram is actually comprised of two independent clusters, indicating that the “humid spots” are subject to different underlying microclimatic mechanism. The hypothesis here is that, since the cold and humid spots are close to the water (Quinnipiac river and the sea), that could be affected by the breeze blowing from the cooler water surface to the warmer land surface, which also brought a large amount of water vapor.

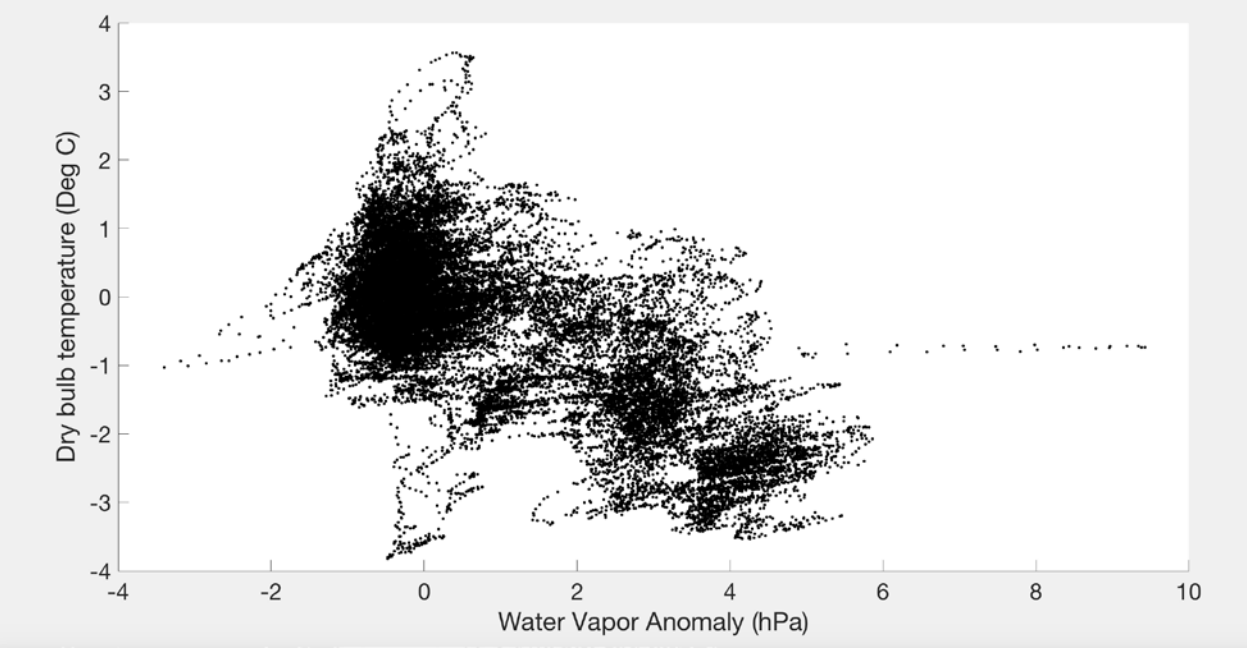

Figure 8. The relationship between the water vapor anomaly and dry bulb temperature.

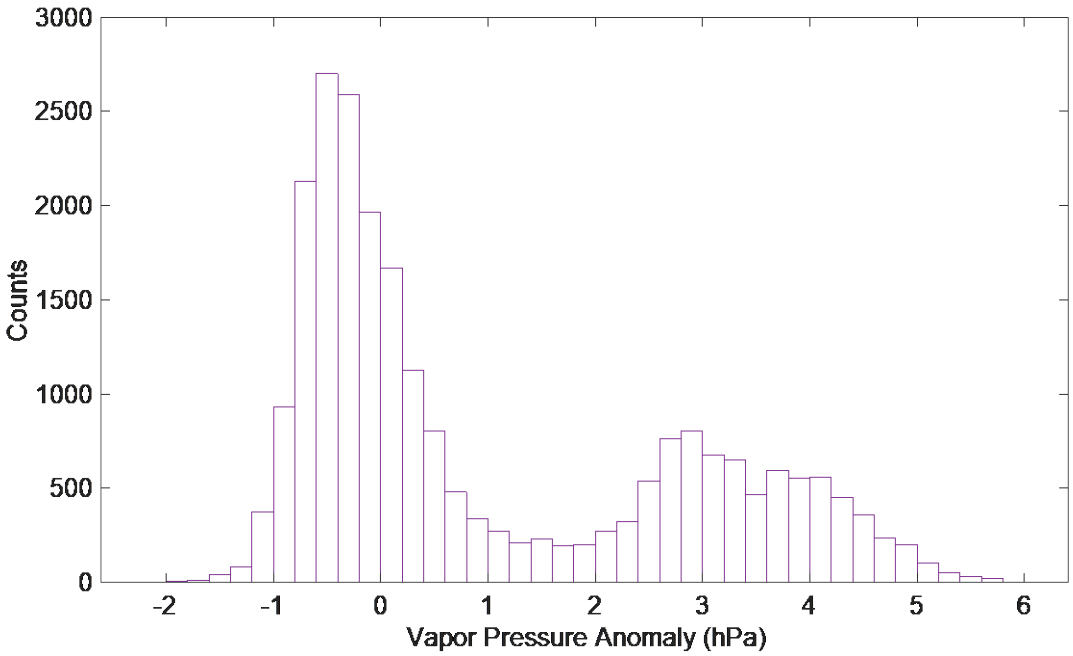

Figure 9. The histogram of vapor pressure anomaly for all the data points on August 12.

By setting a threshold (1.5 hPa) to the vapor pressure anomaly, we can remove all the “abnormal” humid points and only retain the “normal” dry points. Plotting a group of new graphs, we see that now the relationship between AUHI intensity and the environmental indices are more similar for dry bulb temperature and wet bulb temperature (Figure 10).

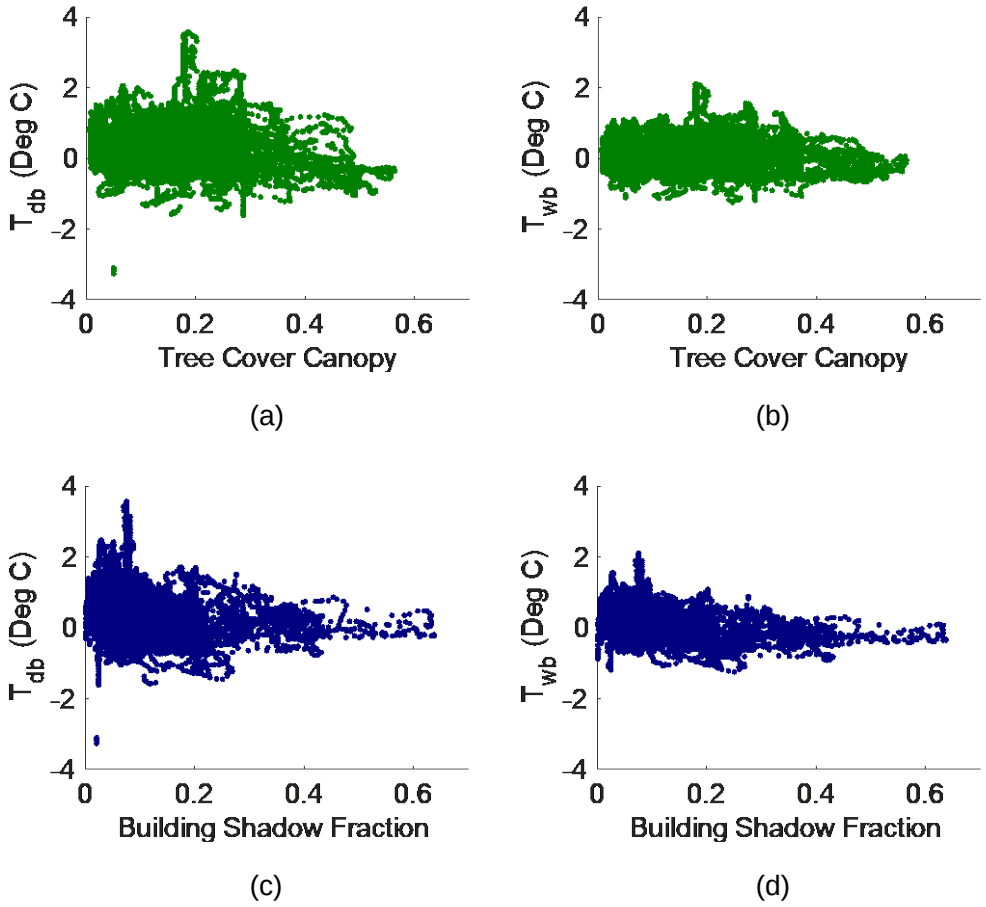

Figure 10. The scatterplot between the environmental indices and the AUHI intensity in terms of dry bulb temperature, (a) and (c), and wet bulb temperature, (b) and (d), for only the drier data points. (a) and (b) are for tree canopy cover, and (c) and (d) are for building shadow fraction.

4.2 The relationship between temperature and moist

Figure 8 provides an intuitional negative correlation between temperature anomaly and humidity anomaly on a typical transect. To understand the correspondence of heat island and wet island effect, we explored a two-dimensional parameter space of dry bulb temperature anomaly and water vapor pressure anomaly. Two typical cluster patterns were discovered for all the transect data (Figure 11). One of the typical patterns in the parameter space contains two main clusters (Figure 11a), with the top-left cluster representing the cold and humid transect data influenced by the sea breeze (humid climate data), and the bottom-right cluster representing the urban area distant to the sea. The other typical pattern only has one main cluster (Figure 11b) controlled by the urban local climate, but still with some outlier points of high humidity that cannot be separated easily.

To separate the transect data regulated by different climatic mechanisms, we built a neural network using the training data from all the transects with a two-cluster pattern, and the data to be predicted

from the rest. The network architecture is comprised of a 6-neuron input layer, a 7-neuron hidden layer, and a simple one-neuron output layer (Figure 12). Six variables, longitude, latitude, temperature anomaly, water vapor anomaly, canopy tree cover, and SVF, have been chosen to be the inputs of the network. Both the input training data and the output data are label with the scheme that the humid climate points are labeled as unreliable (0) and the urban climate points as reliable (1). Finally, we have 9064 unreliable points and 4823 reliable points in the training set. In the training set, 10000 randomly selected points were used for training, and the rest for testing. For the unseen data to be predicted, we have 16816 points. When training the network, we didn't send the training set in sequence. Instead, they were random sampled from the training set for 300,000 times, ensuring that the 10000-size dataset would be used repeatedly to reinforce the weights of the parameters. Since the neural network will output probability values from 0-1, we used a threshold 0.05 to reset the values to 0 and 1. The accuracy is 96.16% for the training set, and 96.30% for the test set.

After doing the prediction on the unseen data, 4737 points were classified as reliable points and 12079 point unreliable. Figure 13 shows the separated plots for all the reliable points and unreliable points, including the points from the training set. The resulting data of urban climate has only one cluster with weak positive correlation between temperature and water vapor anomaly. This indicates that a pure urban area will drive the formation of heat and wet island. On the contrary, the humid climate points show strong negative correlation between temperature and water vapor anomaly. Plotted on the map, humid climate points are noisier than the urban climate points: many abnormal hot spots are on the road without continuity, and the whole transects are affected by the cold and humid sea breeze.

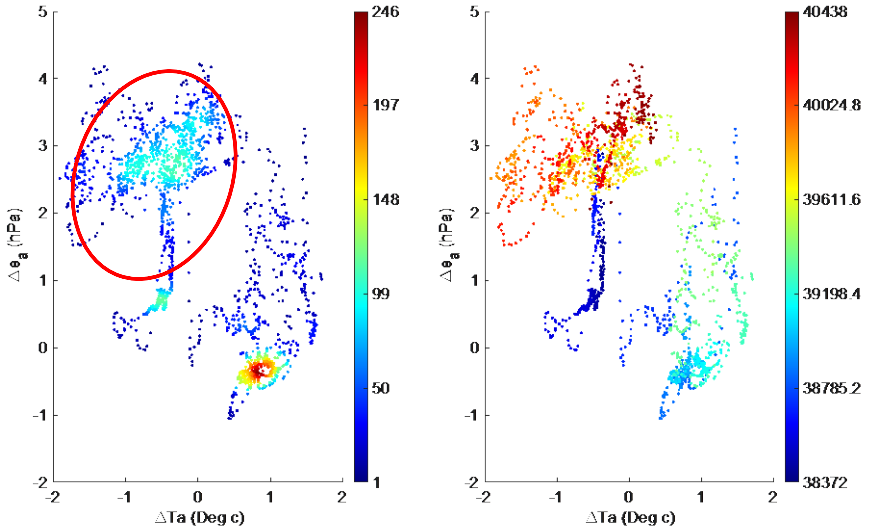

(a)

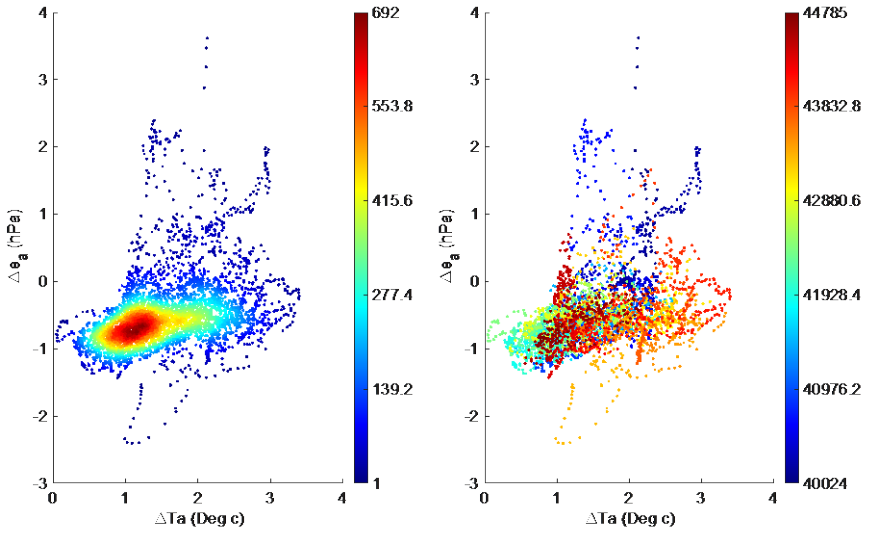

(b)

Figure 11. Two typical examples of the separable transect data and the inseparable transect data. The left panels show the scatter plot of temperature and water vapor anomaly, colorized by the point density to show the clusters. The right panels show the same scatter plot but colorized by time. (a) The data are obviously influenced by the sea breeze (marked by the upper red circle. (b) The data that can't be separated easily because it only has one main cluster.

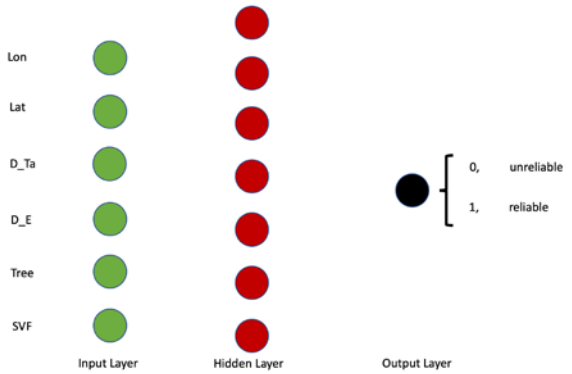

Figure 12. The architecture of my neural network. The green circles are the inputs in the input layer, containing Lon (longiture), Lat (latitude), D_Ta (temperature anomaly), D_E (water vapor anomaly), Tree (street tree cover), and SVF (sky view factor). The red circles represent the hidden layer which has only one more node than the input layer. The output layer has only one node (black circle), giving 0 to indicate unreliable (noise) points, and 1 to indicate reliable (non-noise) points.

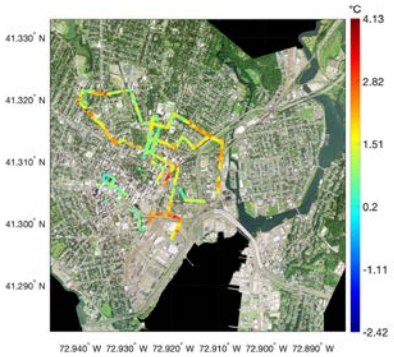

(a)

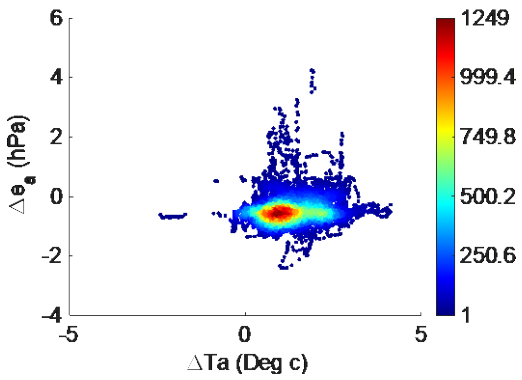

(b)

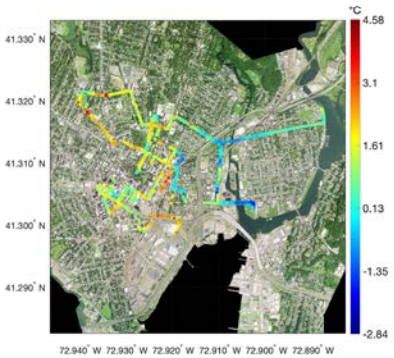

(c)

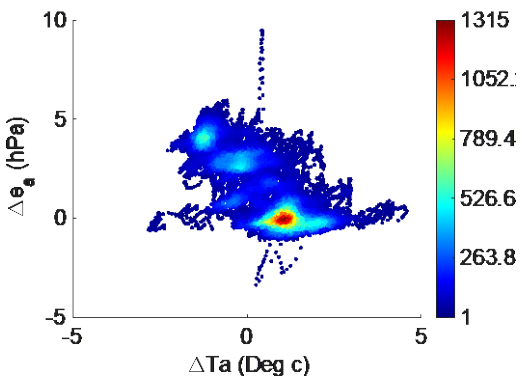

(d)

Figure 13. The merged reliable and unreliable points after prediction. (a) and (b) are the transects plot and scatter plot in the parameter space. (c) and (d) are the similar plots for the unreliable points.

4.3 Characterizing the urban local climate

As the humid climate shows prominent correspondence of heat island and dry island, the urban climate indicates the possibility that a heat island might couple with a wet island. To explore and further characterize the urban climate, additional data transects were analyzed. The data were collected in clear weather condition from September to December, on the same route in the urban area distant to the water body. The time of measurements are from 9 AM to 10 AM when the ocean-land atmospheric circulation was still insignificant. To limit the influence of noise, multiple data transects were averaged to a single transect using inverse-distance weighting. The one-cluster pattern of parameter space shows a stronger positive correlation between temperature and water vapor anomaly (Figure 14). A few outlier points on the top-left correspond with the cold and humid area in the natural park, with dominant tree cover. The results better prove the coupling of heat island and wet island in the urban climate.

With this dataset specialized in local climate, time of a day, and weather, we explored the relationships between the temperature anomaly and tree canopy, building shadow fraction, and SVF (Figure 14). For dry bulb temperature, tree canopy shows stronger cooling effect than we expected from the summer data, a mixture of multiple local climates. Both the building shadow fraction and SVF are negatively correlated with dry bulb temperature. Since higher shadow fraction usually corresponds with lower SVF, the cooling effect of building morphology is solely caused by the reduced incoming solar energy by building blocking. Converting the dry bulb temperature to wet bulb temperature strengthens the climate regulating effect of building morphology. The shadow-related cooling becomes stronger because the urban core with more shadow are usually drier. However, the cooling effect of tree canopy cover becomes insignificant because of the high humidity.

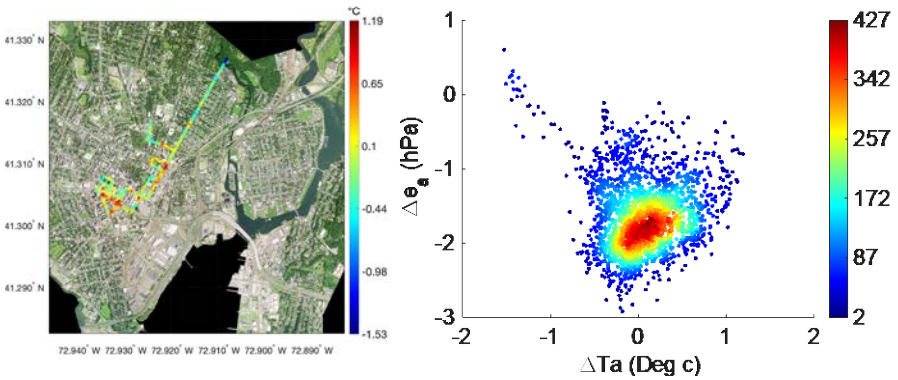

(a) (b)

Figure 13. (a) the averaged dry bulb temperature anomaly for the additional measurements. (b) The cluster plot for the averaged morning data in the urban climate.

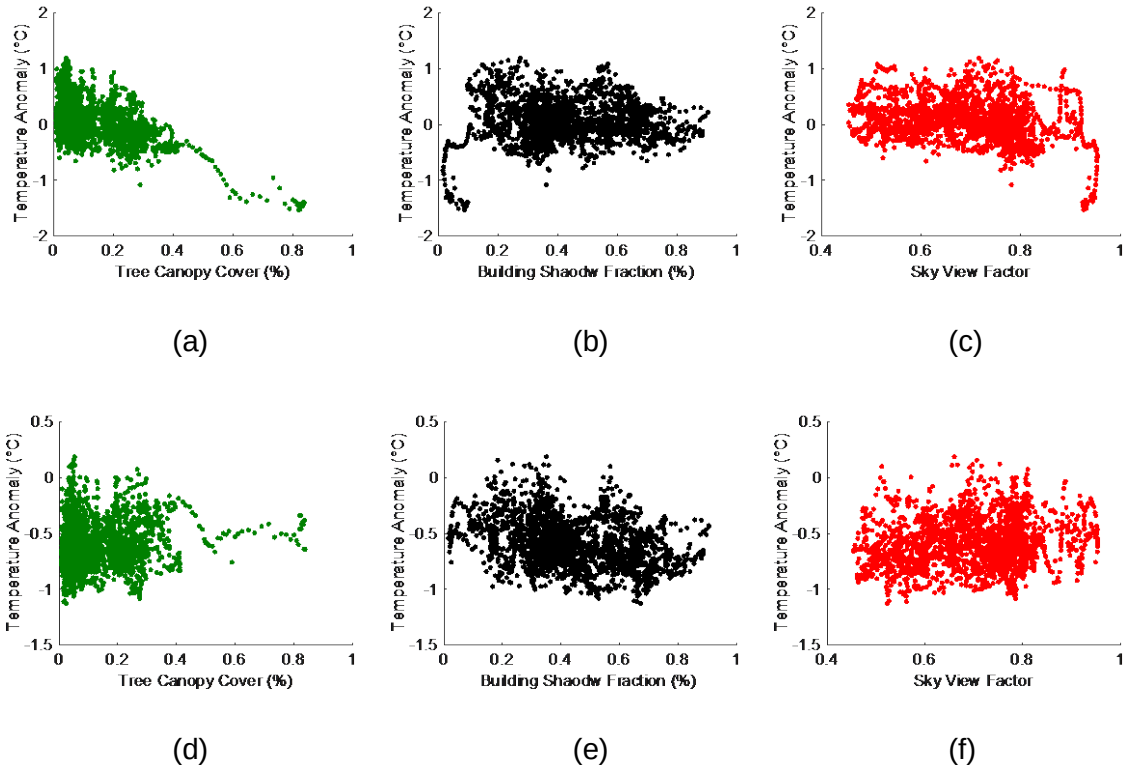

Figure 14. The relationships between temperature anomaly and environmental indices. (a), (b), and (c) are for Tree Canopy Cover, Building Shadow Fraction, and Sky View Factor in terms of dry bulb temperature. (d), (e), and (f) are the corresponding plots for wet bulb temperature.

5. Conclusion

The systematic methodology, mobile measurement, was validated to be useful for collecting data of street level meteorological factors. In terms of the urban landscapes, the tree canopy cover and building shadow fraction have overall cooling effect on both dry bulb and wet bulb temperature. It was found that the measurement in a city can be affected by different local climatic mechanisms. The humid climate, characterized by the effect of daytime sea breeze, has negative correlation between temperature and humidity anomaly: the heat island corresponds with the dry island. On the contrary, a more typical urban climate without the sea breeze shows positive correlation between temperature and humidity anomaly: the heat island corresponds with wet island. The urban area is not persistently drier than the surrounding rural land. For the urban climate, tree canopy cover has

strong cooling effect in terms of dry bulb temperature, while the shadow-related cooling is weaker. In terms of wet bulb temperature, shadow fraction mitigates the UHI the most significantly, while the tree-related cooling becomes trivial.

For the future work, measurements in the different times of a day, different weather conditions will help to clarify the mechanism of UHI formation more profoundly. The reason why the heat island couples with the wet island in a typical urban climate remains to be revealed. This might correspond with additional moist sources in the built-up area, i.e. anthropogenic heat from domestic heating and engine combustion.

6. Reference

[1] IPCC (2014) Climate change 2014: impacts, adaptation, and vulnerability. Part A: global and sectoral aspects. Contribution of working group II to the fifth assessment report of the intergovernmental panel on climate change. Cambridge University Press, Cambridge, United Kingdom and New York, NY, USA.

[2] MedinaRamón M and Schwartz J. Temperature, temperature extremes, and mortality: a study of acclimatisation and effect modification in 50 US cities[J]. *Occupational and environmental medicine*, 2007, 64(12):827–833.

[3] Oleson K W, Monaghan A, Wilhelmi O, et al. Interactions between urbanization, heat stress, and climate change[J]. *Climate Change*, 2015, 129(3-4):525–541.

[4] Peng S, Piao S, Ciais P, et al. Surface urban heat island across 419 global big cities[J]. Environmental Science & Technology, 2012, 46(2):696-703.

[5] Oke T R, Johnson G T, Steyn D G, et al. Simulation of surface urban heat islands under ‘ideal’ conditions at night part 2: Diagnosis of causation[J]. Boundary-Layer Meteorology, 1991, 56(4):339-358.

[6] Carly D. Ziter, Eric J. Pedersen, Christopher J. Kucharik, et al. Scale-dependent interactions between tree canopy cover and impervious surfaces reduce daytime urban heat during summer[J]. PNAS, 2019, https://doi.org/10.1073/pnas.1817561116.

[7] Yokoyama H, Ooka R, Kikumoto H. Study of mobile measurements for detailed temperature distribution in a high-density urban area in Tokyo[J]. Urban Climate, 2017, 24:517-528.

[8] Busato F, Lazzarin R M, Noro M. Three years of study of the Urban Heat Island in Padua: Experimental results[J]. Sustainable Cities & Society, 2014, 10(10):251-258.